



HAL
open science

The impact of the hydrodechlorination process on the physicochemical properties of bimetallic Ag-CuBeta zeolite catalysts

A. Śrębowata, Izabela I. Kamińska, S. Casale, D. Brouri, C. Calers, Stanislaw Dzwigaj

► **To cite this version:**

A. Śrębowata, Izabela I. Kamińska, S. Casale, D. Brouri, C. Calers, et al.. The impact of the hydrodechlorination process on the physicochemical properties of bimetallic Ag-CuBeta zeolite catalysts. *Microporous and Mesoporous Materials*, 2017, 243, pp.56-64. 10.1016/j.micromeso.2016.12.022 . hal-01469231

HAL Id: hal-01469231

<https://hal.sorbonne-universite.fr/hal-01469231v1>

Submitted on 16 Feb 2017

HAL is a multi-disciplinary open access archive for the deposit and dissemination of scientific research documents, whether they are published or not. The documents may come from teaching and research institutions in France or abroad, or from public or private research centers.

L'archive ouverte pluridisciplinaire **HAL**, est destinée au dépôt et à la diffusion de documents scientifiques de niveau recherche, publiés ou non, émanant des établissements d'enseignement et de recherche français ou étrangers, des laboratoires publics ou privés.

The impact of the hydrodechlorination process on the physicochemical properties of bimetallic Ag-CuBeta zeolite catalysts

A. Śrębowata^{1,*}, Izabela I. Kamińska¹, S. Casale², D. Brouri², C. Calers², S. Dzwigaj^{2,*}

¹Institute of Physical Chemistry, Polish Academy of Sciences, Kasprzaka 44/52, 01-224 Warsaw, Poland

²Sorbonne Universités, UPMC Univ Paris 06, CNRS, UMR 7197, Laboratoire de Réactivité de Surface, 4 place Jussieu, F-75252, Paris, France

Figures: 13

*Corresponding authors

Anna Srebowata, E-mail: asrebowata@ichf.edu.pl, Tel. 48 22 343 3320

Stanislaw Dzwigaj, E-mail : stanislaw.dzwigaj@upmc.fr, Fax : 33 1 44 27 21 13

Abstract

Beta zeolites with two Si/Al ratios of 17 and 1300 were used for synthesis of $\text{Ag}_{2.0}\text{Cu}_{2.0}\text{HAlBeta}$ and $\text{Ag}_{2.0}\text{Cu}_{2.0}\text{SiBeta}$ zeolites by conventional wet impregnation and two-step postsynthesis methods, respectively. The calcination of $\text{Ag}_{2.0}\text{Cu}_{2.0}\text{HAlBeta}$ and $\text{Ag}_{2.0}\text{Cu}_{2.0}\text{SiBeta}$ at 773 K for 3 h in air led to formation of C- $\text{Ag}_{2.0}\text{Cu}_{2.0}\text{HAlBeta}$ and C- $\text{Ag}_{2.0}\text{Cu}_{2.0}\text{SiBeta}$. After reduction at 873 K for 3 h in flowing 10 % H_2/Ar , red-C- $\text{Ag}_{2.0}\text{Cu}_{2.0}\text{HAlBeta}$ and red-C- $\text{Ag}_{2.0}\text{Cu}_{2.0}\text{SiBeta}$ were obtained and investigated as the catalysts in gas phase hydrodechlorination of 1,2-dichloroethane at atmospheric pressure, at relatively low reaction temperature (523 K). The state of silver and copper in catalysts at different stages of their biography was characterized by low-temperature N_2 sorption, temperature – programmed reduction (TPR), transmission electron microscopy (TEM), X-ray diffraction (XRD), X-ray photoelectron spectroscopy (XPS), and temperature- programmed hydrogenation (TPH). We have shown that the state of silver and copper species change under HDC conditions. After catalytic run both agglomeration of metal particles and their re-dispersion took place. According to TPH, XRD and XPS measurements we postulate that the cause of this phenomenon is the formation of chlorine containing species in spent zeolite catalysts.

Keywords: Ag, Cu, Beta, hydrodechlorination, 1,2-dichloroethane, physicochemical characterization

1. Introduction

Hydrodechlorination is known as structural sensitive reaction, but among the researchers opinions are divided on the effect of metal(s) dispersion and metal particle size on this process [1,2]. Some of the literature data clearly show the beneficial role of excellent dispersed very small metal particles in the gas - phase hydrodechlorination [2-4]. Our recent studies on nickel containing beta zeolite in conversion of 1,2-dichloroethane brightly demonstrated the high stability, and high selectivity of very small (~1.5 nm) nickel particles [5]. In spite of earlier reports the small metal particles did not deactivate during reaction and they are resistant to sintering [5,6]. As we have earlier shown, the application of dealuminated SiBeta zeolite with vacant T-atom sites played an important role on the formation stable, active and selective catalysts [5,6].

Very interesting results were obtained also for bimetallic Cu-Ni systems prepared by two-step postsynthesis method [7]. Careful investigations have shown very good activity of bimetallic Cu-Ni zeolite catalysts containing small and well dispersed Ni(0) and Cu(0) nanoparticles in hydrodechlorination of 1,2-dichloroethane and high selectivity to ethylene.

Our earlier works [5-8] clearly show that depending on the kind of synthesis method, zeolite catalysts more or less change upon hydrodechlorination conditions. Prepared by two-step postsynthesis method nickel, silver, nickel – silver and nickel - copper containing SiBeta catalysts have shown resistance for changes in aggressive reaction conditions. On the other hand Ni, Ni-Cu, Ag, Ni-Ag containing HAlBeta catalysts synthesized by conventional wet impregnation were more sensitive for sintering and poisoning by carbon and chlorine containing deposits during HDC process [5-8].

Inspired by our earlier works we would like to investigate the effect of two-step postsynthesis method of preparation on catalytic properties of silver and copper loaded bimetallic Beta zeolite catalysts in the hydrodechlorination of 1,2-dichloroethane and

especially on physicochemical properties of zeolite catalysts containing Ag-Cu at various stages of their biographies.

2. Experimental

2.1. Catalysts preparation

A tetraethylammonium Beta (TEABeta) (Si/Al = 17) zeolite provided by RIPP (China) was calcined at 823 K for 15 h in air to remove template. Organic-free HAlBeta zeolite was treated with $13 \text{ mol} \cdot \text{L}^{-1}$ nitric acid (353 K, 4 h) to obtain dealuminated SiBeta zeolite, with Si/Al ratio higher than 1300, and then washed several times with distilled water and dried at 363 K overnight.

$\text{Ag}_{2.0}\text{Cu}_{2.0}\text{HAlBeta}$ and $\text{Ag}_{2.0}\text{Cu}_{2.0}\text{SiBeta}$ were prepared by co-impregnation of 2 g of HAlBeta and SiBEA, respectively, with appropriate concentration of aqueous solutions of AgNO_3 ($c = 3.6 \cdot 10^{-3} \text{ mol L}^{-1}$) and $\text{Cu}(\text{NO}_3)_2$ ($c = 2.2 \cdot 10^{-3} \text{ mol L}^{-1}$). Firstly, both suspensions were stirred for 24 h at 298 K in excess solvent using 200 mL of the precursor solutions. Then, the suspensions were stirred in evaporator under vacuum of a water pump for 2 h in air at 333 K until the water was evaporated. As prepared $\text{Ag}_{2.0}\text{Cu}_{2.0}\text{HAlBeta}$ and $\text{Ag}_{2.0}\text{Cu}_{2.0}\text{SiBeta}$ were further calcined at 773 K for 3 h in static air and labeled C- $\text{Ag}_{2.0}\text{Cu}_{2.0}\text{HAlBeta}$ and C- $\text{Ag}_{2.0}\text{Cu}_{2.0}\text{SiBeta}$, respectively. Then, C- $\text{Ag}_{2.0}\text{Cu}_{2.0}\text{HAlBeta}$ and C- $\text{Ag}_{2.0}\text{Cu}_{2.0}\text{SiBeta}$ were reduced at 873 K, for 3 h in flowing 10% H_2/Ar to obtain red-C- $\text{Ag}_{2.0}\text{Cu}_{2.0}\text{HAlBeta}$ and red-C- $\text{Ag}_{2.0}\text{Cu}_{2.0}\text{SiBeta}$, respectively, where C- stands for calcined and red- for reduced. The catalysts after kinetic run were labeled as spent-red-C- $\text{Ag}_{2.0}\text{Cu}_{2.0}\text{HAlBeta}$ and spent-red-C- $\text{Ag}_{2.0}\text{Cu}_{2.0}\text{SiBeta}$, respectively.

2.2. Catalyst characterization

Specific surface area and adsorption isotherms of nitrogen at 77 K were measured on a Micromeritics ASAP 2020 apparatus, employing the BET (Brunauer-Emmett-Teller) and HK

(Horwath-Kawazoe) methods using nitrogen as adsorbate. Before measuring the adsorption isotherm at 77 K, the samples were kept at 473 K for 4 h in vacuum to remove adsorbed water and gases. The specific surface areas were determined from nitrogen adsorption values from $p/p_0 = 0.05$ to 0.30 using BET method. The maximum pore volume at $p/p_0 = 0.2$ was determined using HK method.

Temperature-programmed reduction for all of the catalysts, after calcination step, was carried out using the glass-flow system. TPR runs were performed in flowing 10 % H₂/Ar (25 cm³ min⁻¹), ramping the temperature at 10 K min⁻¹ and using a Gow-Mac thermal conductivity detector (TCD). Injections of known amounts of hydrogen into the hydrogen–argon flow were provided for calibration (before and after each TPR run).

Catalytic hydrodechlorination of 1,2-dichloroethane (1,2-DCE, HPLC grade, 99.8% pure from Sigma–Aldrich, Germany) was performed at glass flow system at atmospheric pressure, at the temperature of 523 K. The reaction was followed by gas chromatography, using a HP5890 series II gas chromatograph with Flame Ionization Detector (FID), a 5% Fluorcol/Carbopack B column (10 ft) from Supelco. The results of GC analysis were elaborated using HP Chemstation. The total FID signal from the first two analyses was similar to that observed in subsequent GC analyses.

Transmission Electron Microscopy was performed on a JEOL JEM 2100 FEG microscope of the Institut de Mineralogie et de Physique des Milieux Condenses (Université Pierre et Marie Curie) operating at 200 kV, equipped with X-ray energy dispersive spectroscopy for chemical analysis, with 1 nm beam size. Samples were prepared for TEM observations by dispersing the powder ultrasonically in ethanol and depositing a drop on the carbon film. TEM observations were carried out using a Beryllium TEM holder enabling chemical analysis of copper.

X-ray diffractograms for the samples at various stages of their biographies were recorded at room temperature on a PANalytical Empyrean diffractometer using the $\text{CuK}\alpha$ radiation ($\lambda = 154.05 \text{ nm}$).

The X-ray photoelectron spectroscopy measurements were done using an Omicron (ESCA+) X-ray photoelectron spectrometer. The base pressure in the experimental chamber was in the low 10^{-9} mbar range. The spectra were collected using a monochromatic $\text{Al K}\alpha$ ($h\nu = 1486.6 \text{ eV}$) X-ray source with an accelerating voltage of 14 kV and a current intensity of 20 mA. The pass energy was 20 eV for the high resolution spectra and 100 eV for the surveys. Surface charging effects were compensated by referencing the BE (binding energy) to the C 1s line of residual carbon set at 284.7 eV BE.

Temperature-programmed hydrogenation was carried out by mass spectrometry (MA200, Dycor-Ametek, Pittsburgh) to detect a compound that can be removed by hydrogen from spent catalysts. During the experiments, the samples after conversion of 1,2-dichloroethane were heated from $\sim 298 \text{ K}$ to 1073 K in the flow of 20 % H_2/He with ramp rate 10 K min^{-1} and with monitoring of twelve masses (m/z).

3. Results and Discussion

Nitrogen adsorption-desorption isotherms are shown in **Fig. 1**. The open symbols represent adsorption, while the filled ones represent desorption data for the $\text{C-Ag}_{2.0}\text{Cu}_{2.0}\text{SiBeta}$ and $\text{C-Ag}_{2.0}\text{Cu}_{2.0}\text{HAlBeta}$ samples. They exhibit the type I isotherm according to IUPAC [9,10], indicating that they have a microporous structure. All zeolite materials have similar BET surface area and micropore volume (**Table 1**). It is indicating that textural properties of Beta zeolite are preserved upon both methods of their preparation. However, $\text{C-Ag}_{2.0}\text{Cu}_{2.0}\text{HAlBeta}$ zeolite has a little lower specific surface area, probably due to the formation of silver and/or copper oxide that may block access to some pores. Pore size

distribution of C-Ag_{2.0}Cu_{2.0}SiBeta and C-Ag_{2.0}Cu_{2.0}HAIBeta calculated from Horvath-Kawazoe function were shown in **Figure S1** (Supplementary data). The pore volume dependence (cm³ g⁻¹) on the weighted average pore size (nm) is similar in both cases. However, some differences have been observed especially in the case of the smaller pore size.

Temperature-programmed reduction experiments were carried out to determine the reducibility of silver and copper in C-Ag_{2.0}Cu_{2.0}SiBeta and C-Ag_{2.0}Cu_{2.0}HAIBeta zeolites, respectively. As shown in **Fig. 2**, TPR profile for C-Ag_{2.0}Cu_{2.0}SiBeta contains six reduction peaks and the TPR profile for C-Ag_{2.0}Cu_{2.0}HAIBeta contains seven peaks. Comparative study between TPR profiles for C-Ag_{2.0}Cu_{2.0}SiBeta and C-Ag_{2.0}Cu_{2.0}HAIBeta zeolites and TPR profiles for monometallic copper [7] and monometallic silver [11] based on the same zeolite materials (HAIBeta and SiBeta) clearly show an interaction between Ag and Cu. Coexistence of Ag and Cu species leads to the shift of the reduction peaks of silver species toward higher temperatures and copper species toward lower temperatures. Our results are in agreement with earlier studies on bimetallic Ag-Cu species [12]. This effect is clearly seen especially in the case of C-Ag_{2.0}Cu_{2.0}HAIBeta, where two main reduction peaks are observed. One of them, at 468 K, could be assigned to the reduction of Ag species. This maximum is shifted to higher temperature in comparison with the maximum at 466 K for C-Ag_{2.0}HAIBeta [11]. On the other hand, the maximum of the peak at 512 K in case of C-Ag_{2.0}Cu_{2.0}HAIBeta might be attributed to the reduction of copper species. This maximum is significantly shifted to lower temperature, in comparison with the TPR profile for C-Cu_{2.0}HAIBeta [7]. Similarly, the shift of the maximum of the reduction peak toward higher temperatures for silver species and to lower temperatures for copper species is observed in the case of TPR profile for C-Ag_{2.0}Cu_{2.0}SiBeta. This phenomenon confirms the interaction between Cu and Ag, as it was reported earlier [13].

Additional signals in the range of 322-380 K for both zeolite samples could be assigned to the reduction of, existing separately, an excellent dispersed mononuclear Ag(I) and/or silver oxides to metallic Ag⁰ form, in agreement with earlier works on silver based catalysts [14,15]. On the other hand, presence of high temperature peaks, at 711 K in the case of C-Ag_{2.0}Cu_{2.0}HAIBeta and at 692 K in the case of C-Ag_{2.0}Cu_{2.0}SiBeta could be related to the reduction of mononuclear isolated Ag and Cu species. Therefore, we could postulate that independently of the synthesis method, conventional wet impregnation or two-step postsynthesis method, the reduced form of zeolite catalysts contain both monometallic silver and copper nanoparticles and bimetallic Ag-Cu alloys.

As shown in **Fig. 3**, red-C-Ag_{2.0}Cu_{2.0}SiBeta displays very low activity during >1000 minutes of 1,2-dichloroethane hydrodechlorination with conversion less than 1 %. The conversion at the level of ~ 2% is observed only during the first 3 minutes of the reaction. The catalytic behaviour of red-C-Ag_{2.0}Cu_{2.0}SiBeta is very similar to that observed for pure red-C-SiBeta and red-C-Cu_{2.0}SiBeta catalysts [7] and it is in contrast with the results obtained for monometallic red-C-Ag_{2.0}SiBeta catalyst [11]. It means that the coexistence of Cu and Ag does not influence on the increasing of the activity of zeolite materials. However, higher conversion observed after 3 minutes of the reaction could suggest rapid deactivation of red-C-Ag_{2.0}Cu_{2.0}SiBeta under reaction conditions or the catalyst undergoes some equilibration in the initial phase of hydrodechlorination of 1,2-dichloroethane.

In contrast, red-C-Ag_{2.0}Cu_{2.0}HAIBeta exhibits higher than 6 % of 1,2-DCE conversion after 16 h of reaction. For this zeolite catalyst the activation takes place during the first 100 min. of 1,2-DCE hydrodechlorination and afterwards slow deactivation is observed (**Fig. 3**). The similar results obtained for red-C-Ag_{2.0}Cu_{2.0}HAIBeta and pure red-C-HAIBeta [7] display lower activity and higher stability of bimetallic Ag-Cu catalyst. It could indicate that the state of bimetallic Ag-Cu species has changed under reaction conditions.

The application of both red-C-Ag_{2.0}Cu_{2.0}SiBeta and red-C-Ag_{2.0}Cu_{2.0}HAIBeta in HDC reaction leads to formation of desired product of 1,2-dichloroethane hydrodechlorination such as ethylene and vinyl chloride (**Figs 4 and 5**). Although the coexistence of Ag and Cu in red-C-Ag_{2.0}Cu_{2.0}SiBeta does not affect the activity of catalyst, it is visible in the product distribution. During the first minutes of the reaction ~ 50 % of C₂H₄ and ~ 50 % of C₂H₃Cl were formed in the case of red-C-Ag_{2.0}Cu_{2.0}SiBeta, while 100 % of vinyl chloride is observed for red-C-SiBeta [7]. Additionally, the selectivity toward ethylene increased during the time at the expense of the selectivity to vinyl chloride. After 1000 minutes of the reaction the selectivity to ethylene was 74 % and to vinyl chloride 26 % (**Figs. 4 and 5**). This phenomenon confirms our suppositions that the catalyst surface is modified under HDC 1,2-dichloroethane conditions. However, in the case of red-C-Ag_{2.0}Cu_{2.0}HAIBeta the presence of Ag and Cu does not affect the selectivity toward products of 1,2-dichloroethane hydrodechlorination. Red-C-Ag_{2.0}Cu_{2.0}HAIBeta alike of red-C-HAIBeta shows ~ 100 % selectivity toward vinyl chloride [7]. It could suggest that the presence of both Brønsted and Lewis acidic sites plays an important role in catalytic behaviour of red-C-Ag_{2.0}Cu_{2.0}HAIBeta catalyst.

TEM measurements were carried out for red-C-Ag_{2.0}Cu_{2.0}SiBeta, red-C-Ag_{2.0}Cu_{2.0}HAIBeta, spent-red-C-Ag_{2.0}Cu_{2.0}SiBeta and spent-red-C-Ag_{2.0}Cu_{2.0}HAIBeta. The correlation of the samples composition and nanoparticles sizes leads to classify particles in two categories (**Figs 6-9**):

- i) small bimetallic nanoparticles slightly monodisperse in size (5 nm for red-C-Ag_{2.0}Cu_{2.0}HAIBeta and 3 nm for red-C-Ag_{2.0}Cu_{2.0}SiBeta) but with heterogeneous composition (from 20 % to 95 % of Ag).
- ii) larger nanoparticles, heterogeneous in size (from 10 to 50 nm) in the case of red-C-Ag_{2.0}Cu_{2.0}HAIBeta and red-C-Ag_{2.0}Cu_{2.0}SiBeta) but with homogenous composition (95 % Ag).

The presence of large monometallic silver nanoparticles are in agreement with XRD results too.

In the case of spent-red-C-Ag_{2.0}Cu_{2.0}HAIBeta, additional third category of nanoparticles was observed. Monometallic copper small nanoparticles with an average particles diameter from 2 to 5 nm were found. It seems that small copper nanoparticles were formed by aggregation of very small copper clusters that could not be observed for red-C-Ag_{2.0}Cu_{2.0}HAIBeta due to resolution limits of the microscope.

On the other hand, in the case of red-C-Ag_{2.0}Cu_{2.0}HAIBeta we could observe only one category of slightly monometallic (95 % Ag) nanoparticles with diameters from 3 nm to 50 nm. It seems that bimetallic nanoparticles lost Cu and became Ag nanoparticles. We can think also that very small Cu nanoparticles (diameter < 2 nm) were formed but could not be observed due to instrumental resolution limitation.

The effect of re-dispersion of active phase under HDC conditions is indicated especially for noble metals such as Pt and Pd [16,17]. This phenomenon is usually explained by the formation, volatilisation and re-deposition of unstable metallic chlorides resulting from the reaction between metallic particle and HCl [16-18]. In agreement with earlier study of Fung and Sinfelt [19], concerning the hydrogenolysis of methyl chloride CH₃Cl on metals from group IB, they are able to form a metal-chlorine bond, as demonstrated by the existence of stable chlorides.

Consequently, the formation of smaller metal particles could lead to a stronger reactant-surface interaction, and therefore to an increase in the selectivity for more dechlorinated molecule. Therefore, during 1,2-dichloroethane hydrodechlorination on red-C-Ag_{2.0}Cu_{2.0}SiBeta gradual increasing of the selectivity to ethylene was observed (**Fig. 4**), at the expense of decreasing selectivity toward vinyl chloride (**Fig. 5**). In this way, hydrodechlorination is considered as structure-sensitive reaction [6,16,17].

On the other hand, the formation of volatile metallic chlorides, such as Cu_xCl_y could lead to their migration and re-dispersion of active phase [19,20]. The reduction of chlorides by the hydrogen introduced as reactant could lead to formation of much smaller metal particles [20]. These phenomena could be the reason of disappearance of Cu in TEM images for spent zeolite catalysts.

Figs. 10 and **11** show the XRD results for both zeolite HAlBeta and SiBeta supports and for Ag-Cu containing HAlBeta and SiBeta catalysts on different stages of their biography (for as prepared, reduced and spent samples). They are characterized by high crystallinity and correspond to Beta-type zeolite structure. It indicates that calcination (at 823 K during 15 h), dealumination with nitric acid, reduction at 873 K during 3 h and hydrodechlorination processes did not affect crystallinity of the zeolite catalysts.

Moreover, as prepared Ag and Cu loaded zeolite samples do not show any evidence of extra-framework compound or amorphization of the zeolite, indicating good dispersion of nickel and copper in zeolite structure. A change of the position of the narrow main diffraction peak around 2θ of 22.60° , generally taken as evidence of framework contraction/expansion of BEA structure, from 22.54° for HAlBeta to 22.46° for $\text{Ag}_{2.0}\text{Cu}_{2.0}\text{HAlBeta}$ and from 22.86° for SiBeta to 22.59° for $\text{Ag}_{2.0}\text{Cu}_{2.0}\text{SiBeta}$ indicates matrix expansion and incorporation of metals ions into the framework of Beta zeolite (**Figs. 10** and **11**). For red-C- $\text{Ag}_{2.0}\text{Cu}_{2.0}\text{HAlBeta}$ (**Fig. 10**) and red-C- $\text{Ag}_{2.0}\text{Cu}_{2.0}\text{SiBeta}$ (**Fig. 11**) additional phase of Ag is observed suggesting sintering and formation of big monometallic silver crystallites after reduction step. These XRD results are in agreement with the data obtained for TEM measurements.

Catalytic conversion of 1,2-dichloroethane involves additional changes in the structure of the zeolite catalysts. They contain additionally reflexes related to AgCl and CuCl_2 salts (**Figs 10** and **11**) which is a signature of the formation and agglomeration of silver and copper chlorine in both catalysts. This could be the reason of rapid deactivation of these catalysts

during hydrodechlorination of 1,2-dichloroethane, as it was reported earlier for silver and copper containing catalysts in HDC process [7,11].

In the C 1s XP spectra of red-C-Ag_{2.0}Cu_{2.0}HAIBeta, spent-red-C-Ag_{2.0}Cu_{2.0}HAIBeta, red-C-Ag_{2.0}Cu_{2.0}SiBeta and spent-red-C-Ag_{2.0}Cu_{2.0}SiBeta there are three main contributions at 284.7, 285.8 - 286.0 and 287.0 - 287.5 eV, corresponding respectively to i) C-C and C-H, ii) C-O and C-N and iii) C=O bindings (results not shown). In the O 1s spectra of these samples, one peak is observed at c.a. 532.7 - 533.7 eV (result not shown) that is attributed to Si-O-Si bond [21]. The Si 2p spectra for all tested samples exhibit a peak at c.a. 103.5 - 104.5 eV (results not shown) related to energy binding of Si 2p present in the structure of zeolite [22].

XPS was used to determine the valence state of the silver and copper species in red-C-Ag_{2.0}Cu_{2.0}HAIBeta, spent-red-C-Ag_{2.0}Cu_{2.0}HAIBeta, red-C-Ag_{2.0}Cu_{2.0}SiBeta and spent-red-C-Ag_{2.0}Cu_{2.0}SiBeta. **Figure S2** shows the Ag 3d_{3/2} and 3d_{5/2} bands of red-C-Ag_{2.0}Cu_{2.0}HAIBeta and spent-red-C-Ag_{2.0}Cu_{2.0}HAIBeta. Binding energies (BE) of Ag 3d_{5/2} (369 eV) and Ag 3d_{3/2} (375 eV) for spent-red-C-Ag_{2.0}Cu_{2.0}HAIBEA differ slightly (0.5 eV) from the BE observed for red-C-Ag_{2.0}Cu_{2.0}HAIBeta (368.5 and 374.5 eV). The increase of the binding energy of Ag 3d bands after hydrodechlorination of 1,2-dichloroethane on red-C-Ag_{2.0}Cu_{2.0}HAIBeta could indicate oxidation of silver upon this reaction.

The Cu 2p XPS spectrum of red-C-Ag_{2.0}Cu_{2.0}HAIBeta and spent-red-C-Ag_{2.0}Cu_{2.0}HAIBeta is deconvoluted into two doublets (**Fig. S3**). In the 2p_{3/2} range the most intensive peak appears at 933.7 - 933.5 eV and the second peak at 936.5 - 935.8 eV. Both peaks are characteristic of Cu(II), first one probably of well dispersed pseudo-tetrahedral Cu(II) and the second one of octahedrally coordinated Cu(II), in line with earlier reports [23, 24]. In the 2p_{1/2} range the most intensive peak appears at 953.6 - 953.3 eV and the second one at 956.5 - 956 eV (**Fig. S3**). Absence of satellite peaks which could be identified to Cu(II) is

probably due to very high dispersion and strong interaction of Cu(II) ions with zeolite matrix, in line with earlier reports [23, 24].

In the case of red-C-Ag_{2.0}Cu_{2.0}SiBeta and spent-red-C-Ag_{2.0}Cu_{2.0}SiBeta BE of Ag 3d_{5/2} and Ag 3d_{3/2} are very close and equal 369.1 - 369.0 and 375.1 - 375.0 eV, respectively (**Fig. S4**). XPS results show that BE of Ag 3d_{5/2} and Ag 3d_{3/2} do not change during hydrodechlorination of 1,2-dichloroethane on red-C-Ag_{2.0}Cu_{2.0}SiBeta.

In the case of red-C-Ag_{2.0}Cu_{2.0}SiBeta and spent-red-C-Ag_{2.0}Cu_{2.0}SiBeta BE of Cu 2p peaks appears as two doublets in the 2p_{1/2} and 2p_{3/2} ranges (**Fig. S5**). In the 2p_{3/2} range the most intensive peak appears at 934.9 - 933.6 eV and the second peak at 937.1 - 935.9 eV. Both peaks are characteristic of Cu(II), first one probably of well dispersed pseudo-tetrahedral Cu(II) and the second one of octahedrally coordinated Cu(II), in line with earlier reports [23,24]. In the 2p_{1/2} range the most intensive peak appears at 954.8 - 954.0 eV and the second one at 957.1 - 956.4 eV (**Fig. S5**). Moreover, according to Yea et al. [25], the presence of Cu(II) species can be confirmed by appearance of shake-up satellite peaks at 942.2 - 945.0 and 962.3 - 964.3 eV, characteristic of Cu(II) species and they evidence of an open 3d⁹ shell [26, 27].

Very interesting information follows from the TPH (temperature – programmed hydrogenation) of deposit retained by the spent-red-C-Ag_{2.0}Cu_{2.0}SiBeta and spent-red-C-Ag_{2.0}Cu_{2.0}HAIBeta. During hydrodechlorination of 1,2-dichloroethane on Ag-Cu catalysts both carbon and chlorine species were formed. Significant differences observed for spent-red-C-Ag_{2.0}Cu_{2.0}HAIBeta and spent-red-C-Ag_{2.0}Cu_{2.0}SiBeta were shown by the representative data obtained for the *m/z* 15 (CH₄), *m/z* 28 (C₂H_x) and *m/z* 62 (C₂H_xCl) and *m/z* 36 (HCl) respectively (**Figs 12 and 13**). Comparison study between both spent Ag-Cu catalysts suggests negligible amounts of carbonaceous species on spent-red-C-Ag_{2.0}Cu_{2.0}SiBeta and significant amounts of carbonaceous species on spent-red-C-Ag_{2.0}Cu_{2.0}HAIBeta. Additionally, very high

temperature (> 800 K) needs for the removal of these deposits from catalyst surface, suggests a very strong interaction between deposits and the spent-red-C-Ag_{2.0}Cu_{2.0}HAIBeta surface. This phenomenon could suggest the carburization of the Brønsted and Lewis acidic sites under reaction conditions.

HCl (m/z 36) (**Figs 12 and 13**) liberation for spent-red-C-Ag_{2.0}Cu_{2.0}SiBeta and spent-red-C-Ag_{2.0}Cu_{2.0}HAIBeta means that the accumulation of chlorine species on both these catalysts during HDC process is strongly related to the presence of Ag and Cu metals. Evolution of m/z 62 for both catalysts confirms the formation of deposits containing both carbon and chlorine.

TPH results obtained for spent-red-C-Ag_{2.0}Cu_{2.0}HAIBeta and spent-red-C-Ag_{2.0}Cu_{2.0}SiBeta are in agreement with our earlier studies for nickel containing Beta zeolite [6].

4. Conclusions

The investigation realized in this work clearly shows that the two-step postsynthesis method leads to the formation mainly very small, Ag and Cu nanoparticles in reduced form of the catalyst.

Application of red-C-Ag_{2.0}Cu_{2.0}HAIBeta catalyst in 1,2-dichloroethane hydrodechlorination gives almost 100 % selectivity into vinyl chloride, desired product of this reaction, in contrast, application of red-C-Ag_{2.0}Cu_{2.0}SiBeta gives ethylene as a main product which is second desired products of this reaction.

Under HDC process on the both catalysts carbon and chlorine species are deposited. We have shown that Ag and Cu nanoparticles agglomerate and transform into AgCl and CuCl₂.

Acknowledgement

I.I. Kamińska and A. Śrębowata would like to thank the Institute of Physical Chemistry PAS in Warsaw for the financial support.

References

1. M.A. Kean, *ChemCatChem*, 3 (2011), 800-821.
2. D. Comandella, S. Woszdlo, A. Georgi, F.D. Kopinke, K. Mackenzie, *Appl. Catal. B* 186 (2016) 204-211.
3. M.Martin-Martinez, L.M.Gómez-Sainero, J.Bedia, A.Arevalo-Bastante, J.J.Rodriguez, *Appl. Catal. B* 184 (2016) 55-63.
4. M. Bonarowska, Z. Karpiński, R. Kosydar, T. Szumelda, A. Drelinkiewicz, C. R. *Chim.* 18 (2015) 1143-1151.
5. R. Baran, I.I. Kamińska, A. Śrębowata, S. Dzwigaj, *Micropor. Mesopor. Mater.* 169 (2013) 120–127.
6. A. Śrębowata, R. Baran, D. Łomot, D. Lisovytskiy, T. Onfroy, S. Dzwigaj, *Appl. Catal. B* 147 (2014) 208–220.
7. A. Śrębowata, R. Baran, S. Casale, I.I. Kamińska, D. Łomot, D. Lisovytskiy, S. Dzwigaj, *Appl. Catal. B* 152–153 (2014) 317–327.
8. A. Śrębowata, I. Zielińska, R. Baran, G. Słowik, S. Dzwigaj, *Catal. Commun.* 69 (2015) 154–160.
9. IUPAC Recommendations, *Pure Appl. Chem.*, 1985, 57, 603–619
10. IUPAC Recommendations, *Pure Appl. Chem.*, 1994, 66, 1739–1758
11. A. Śrębowata, R. Baran, G. Słowik, D. Lisovytskiy, S. Dzwigaj, *Appl. Catal. B* 199 (2016) 514–522.

12. D. Sun, Y. Yamada, S. Sato, *Appl. Catal. A* 475 (2014) 63–68.
13. X. Zheng, Q. Zhang, Y. Guo, W. Zhan, Y. Guo, Y. Wang, G. Lu, *J. Mol. Catal.* 357 (2012) 106–111.
14. N. Popovych, P. Kyriienko, S. Soloviev, S. Orlyk, S. Dzwigaj, *Micropor. Mesopor. Mater.* 203 (2015) 163–169.
15. D. Chen, Z. Qu, S. Shen, X. Li, Y. Shi, Y. Wang, Q. Fu, J. Wu, *Catal. Today* 175 (2011) 338–345.
16. M.A. Álvarez-Montero, L.M. Gómez-Sainero, A. Mayoral, I. Diaz, R.T. Baker, J.J. Rodriguez, *J. Catal.* 279 (2011) 389–396.
17. S. Ordóñez, F. V. Diez, H. Sastre, *Appl. Catal. B* 31 (2001) 113–122.
18. K. Fogar, D. Hay, H. Jaeger, *J. Catal.* 96 (1985) 154–169.
19. S.C. Fung, J.H. Sinfelt, *J. Catal.* 103 (1987) 220–223.
20. M. Martin-Martinez, L.M. Gómez-Sainero, M.A. Alvarez-Montero, J. Bedia, J.J. Rodriguez, *Appl. Catal.* 132–133 (2013) 256–265.
21. D. Zhang, Y. Wei, L. Xu, F. Chang, Z. Liu, S. Meng, B.-L. Su, Z. Liu, *Micropor. Mesopor. Mater.* 116 (2008) 684–692.
22. D. Esquivel, A. J. Cruz-Cabeza, C. Jimenez-Sanchidrian, F.J. Romero-Salguero, *Micropor. Mesopor. Mater.* 142 (2011) 672–679.
23. S. Dzwigaj, J. Janas, J. Mizera, J. Gurgul, R.P. Socha, M. Che, *Catal. Lett.* 126 (2008) 36–42.
24. J. Janas, J. Gurgul, R.P. Socha, S. Dzwigaj, *Appl. Catal. B* 91 (2009) 217–224.
25. Q. Yea, L. Wanga, R.T. Yanga, *Appl. Catal. A* 427–428 (2012) 24–34.
26. X. Li, X. Zhang, L. Lei, *Separ Purif Technol.* 64 (2009) 326–331.
27. M. Zahmakıran, F. Durap, S. Ozkar, *Int. J. Hydrogen Energy* 35 (2010) 187–197.

Table 1. Specific surfaces area, pore volume and weighted average pore size determined from the nitrogen adsorption–desorption isotherms of calcined zeolite catalysts.

Sample	Specific surface area ^a (m ² g ⁻¹)	Pore volume ^b (cm ³ g ⁻¹)	Weighted average pore size ^b (nm)
C-Ag _{2.0} Cu _{2.0} SiBeta	333	0.14	1.53
C-Ag _{2.0} Cu _{2.0} HAIBeta	303	0.13	1.49

^a calculated from BET isotherms

^b calculated from Horvath-Kawazoe function

Figure captions

Figure 1. Adsorption and desorption isotherms of N₂ at 77 K for calcined C-Ag_{2.0}Cu_{2.0}SiBeta and C-Ag_{2.0}Cu_{2.0}HAIBeta. Empty symbols: adsorption; filled symbols: desorption.

Figure 2. TPR patterns of C-Ag_{2.0}Cu_{2.0}SiBeta and C-Ag_{2.0}Cu_{2.0}HAIBeta.

Figure 3. Time-on-stream behavior in hydrodechlorination of 1,2-DCE on red-C-Ag_{2.0}Cu_{2.0}SiBeta and red-C-Ag_{2.0}Cu_{2.0}HAIBeta catalysts at 523 K: overall conversion.

Figure 4. Time-on-stream behavior in hydrodechlorination of 1,2-DCE on red-C-Ag_{2.0}Cu_{2.0}SiBeta and red-C-Ag_{2.0}Cu_{2.0}HAIBeta catalysts at 523 K: ethylene selectivity.

Figure 5. Time-on-stream behavior in hydrodechlorination of 1,2-DCE on red-C-Ag_{2.0}Cu_{2.0}SiBeta and red-C-Ag_{2.0}Cu_{2.0}HAIBeta catalysts at 523 K: vinyl chloride selectivity.

Figure 6. Bright field TEM micrographies of bimetallic red-C-Ag_{2.0}Cu_{2.0}HAIBeta (up) and spent-red-C-Ag_{2.0}Cu_{2.0}HAIBeta (down) and XEDS spectra of representative nanoparticles.

Figure 7. Bright field TEM micrographies of bimetallic red-C-Ag_{2.0}Cu_{2.0}SiBeta (up) and spent-red-C-Ag_{2.0}Cu_{2.0}SiBeta (down) and XEDS spectra of representative nanoparticles.

Figure 8. Correlation diagram for composition and size of nanoparticles for red-C-Ag_{2.0}Cu_{2.0}HAIBeta (up) and spent-red-C-Ag_{2.0}Cu_{2.0}HAIBeta (down).

Figure 9. Correlation diagram for composition and size of nanoparticles for red-C-Ag_{2.0}Cu_{2.0}SiBeta (up) and spent-red-C-Ag_{2.0}Cu_{2.0}SiBeta (down).

Figure 10. XRD results for SiBeta, as prepared Ag_{2.0}Cu_{2.0}SiBeta, red-C-Ag_{2.0}Cu_{2.0}SiBeta and spent-red-C-Ag_{2.0}Cu_{2.0}SiBeta (x – Ag(0), circles – AgCl, stars – CuCl₂).

Figure 11. XRD results for HAIBeta, as prepared Ag_{2.0}Cu_{2.0}HAIBeta, red-C-Ag_{2.0}Cu_{2.0}HAIBeta and spent-red-C-Ag_{2.0}Cu_{2.0}HAIBeta (x – Ag(0), circles – AgCl, stars – CuCl₂).

Figure 12. TPH profiles for spent-red-C-Ag_{2.0}Cu_{2.0}SiBeta catalyst after hydrodechlorination of 1,2-DCE.

Figure 13. TPH profiles for spent-red-C-Ag_{2.0}Cu_{2.0}HAIBeta catalyst after hydrodechlorination of 1,2-DCE.

ACCEPTED MANUSCRIPT

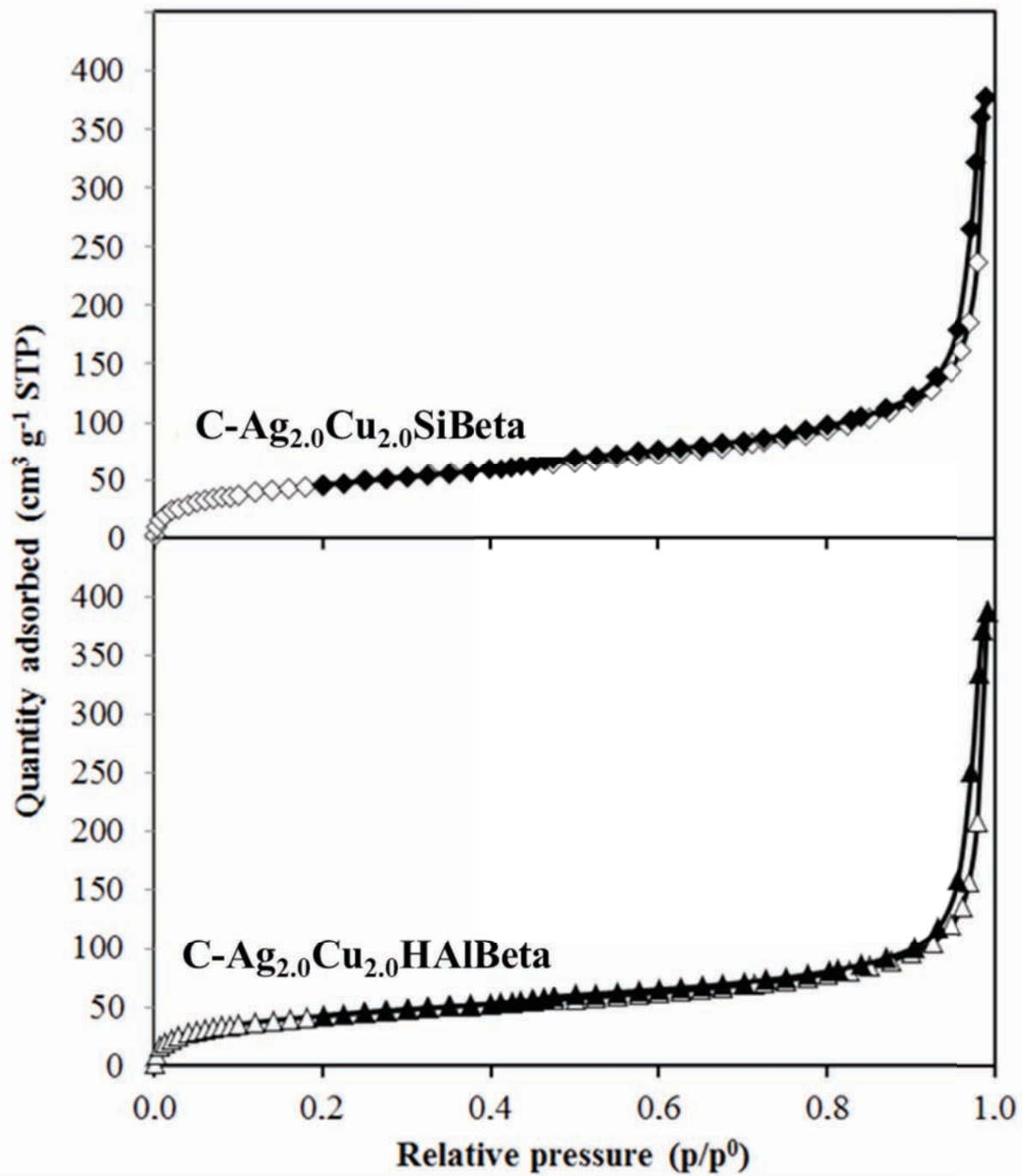


Figure 1

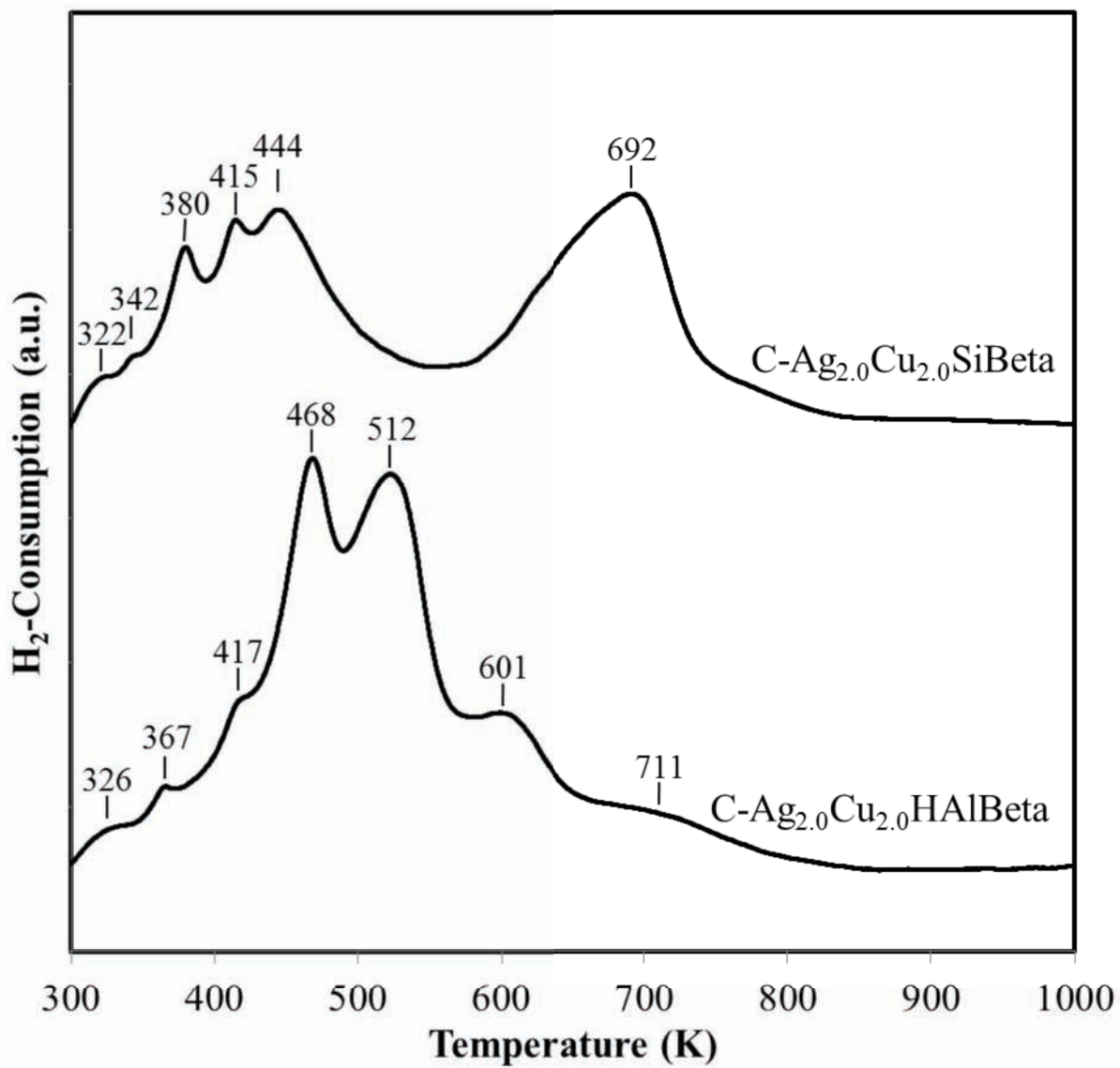


Figure 2

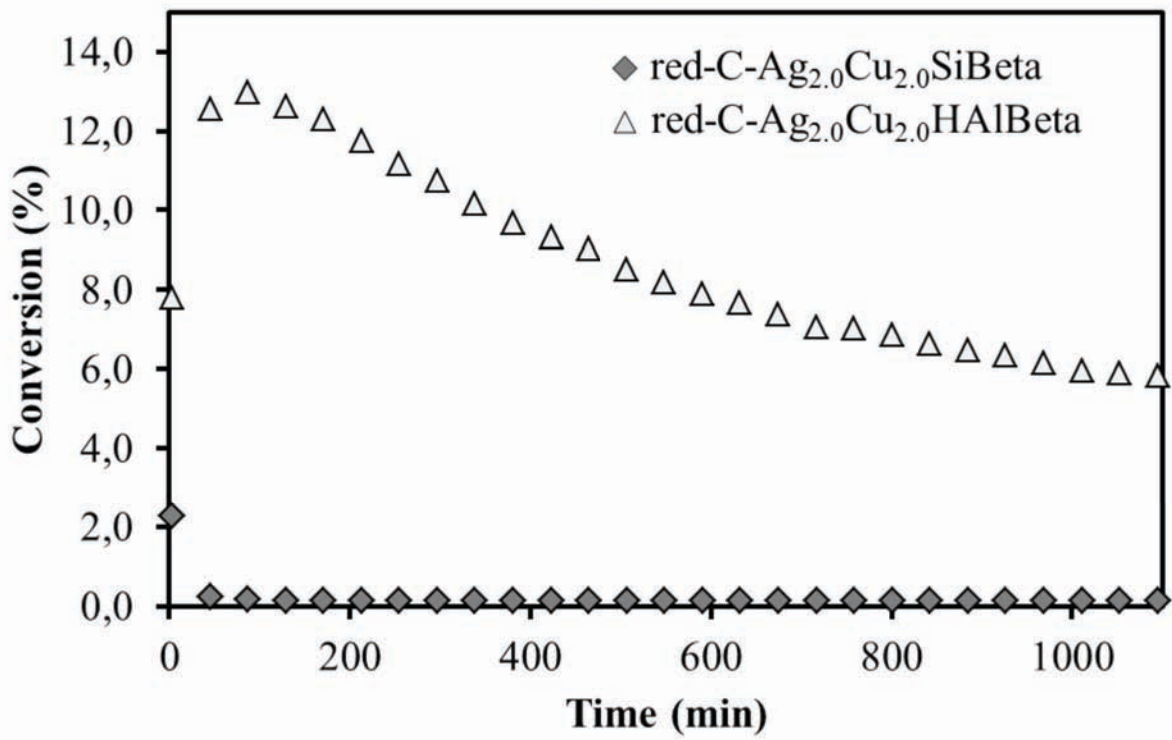


Figure 3

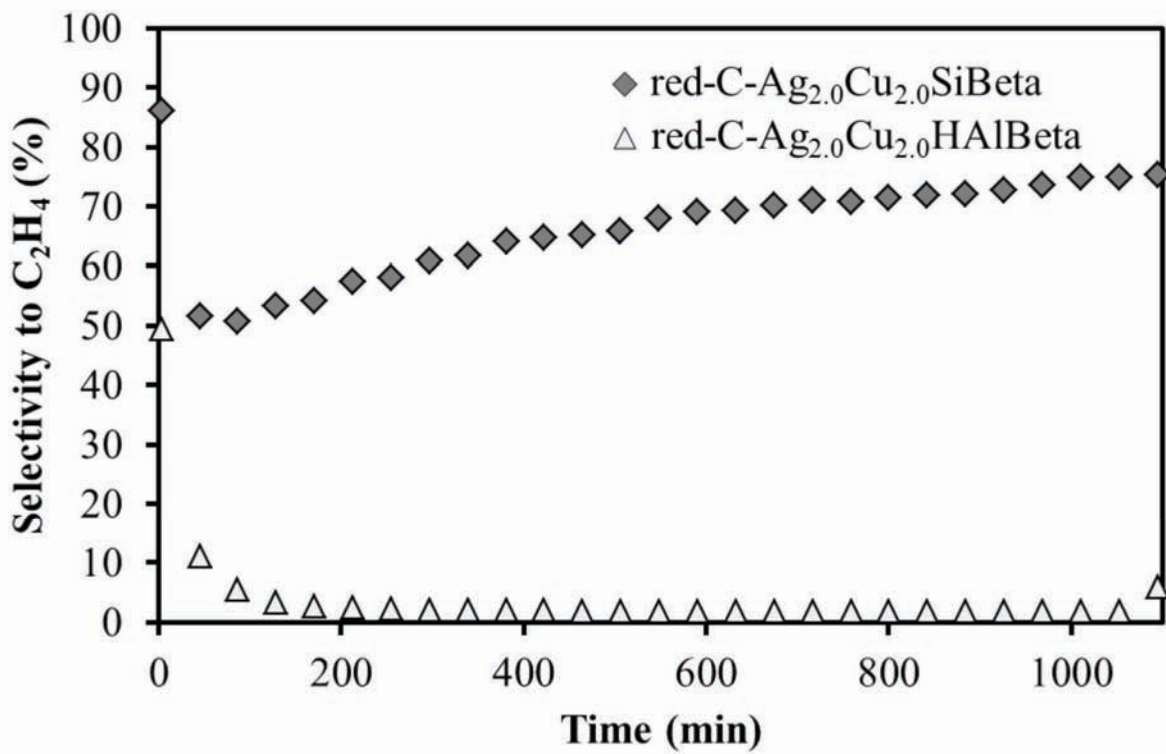


Figure 4

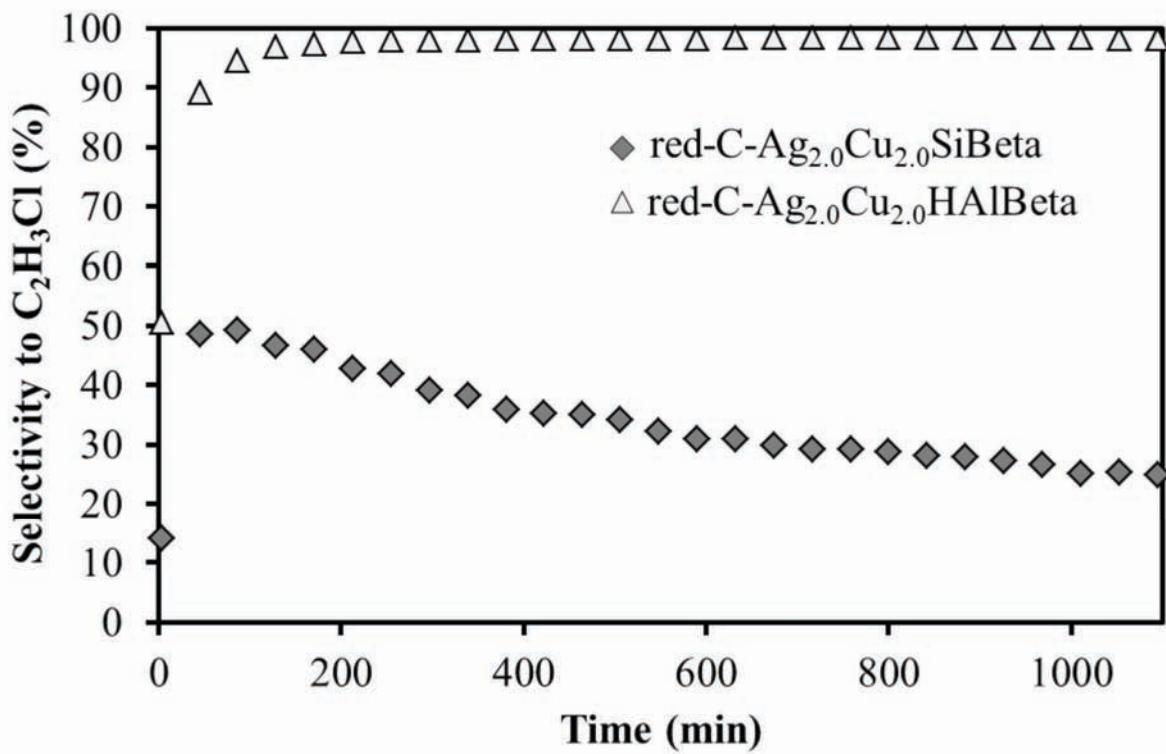


Figure 5

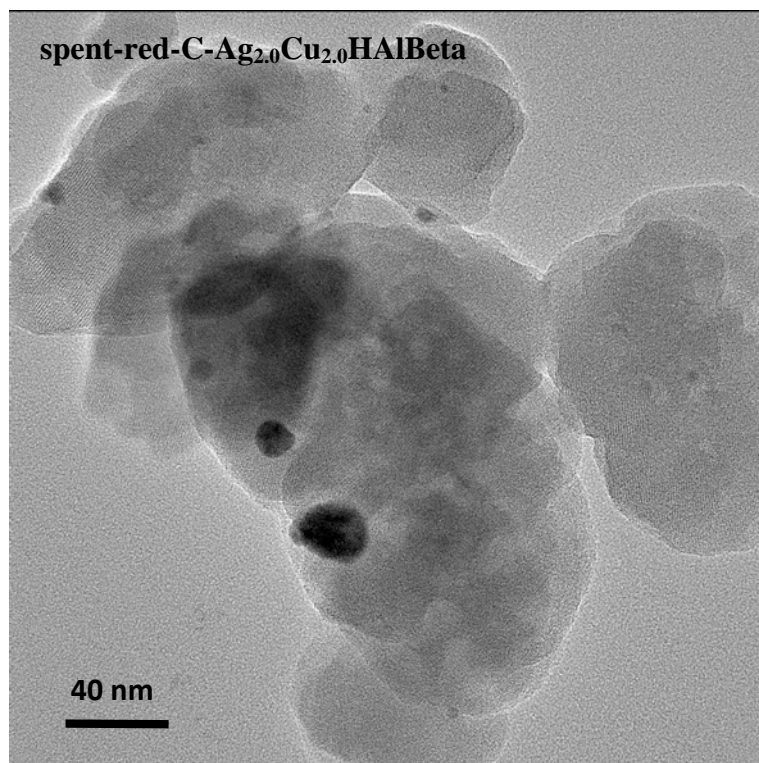
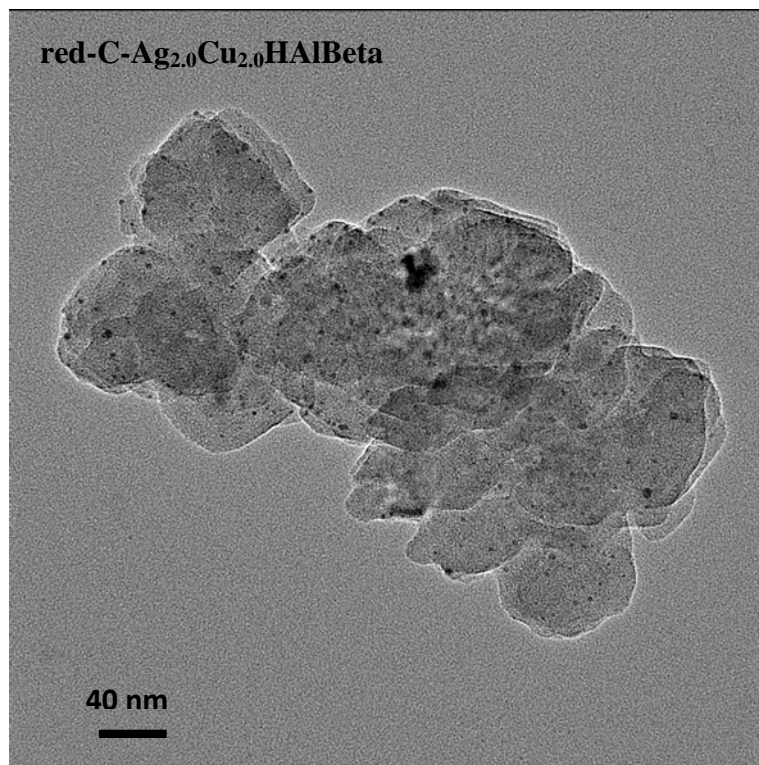


Figure 6

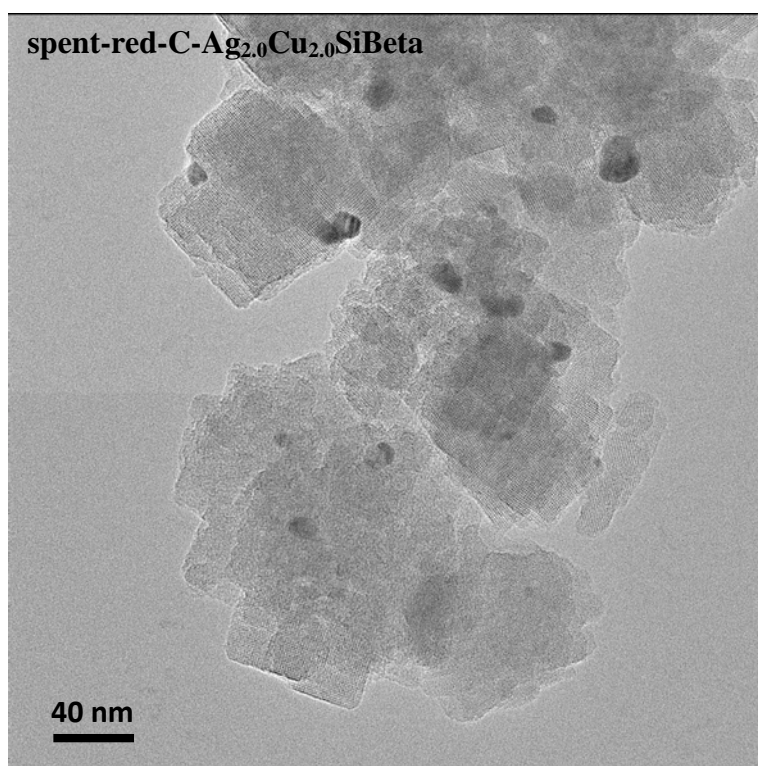
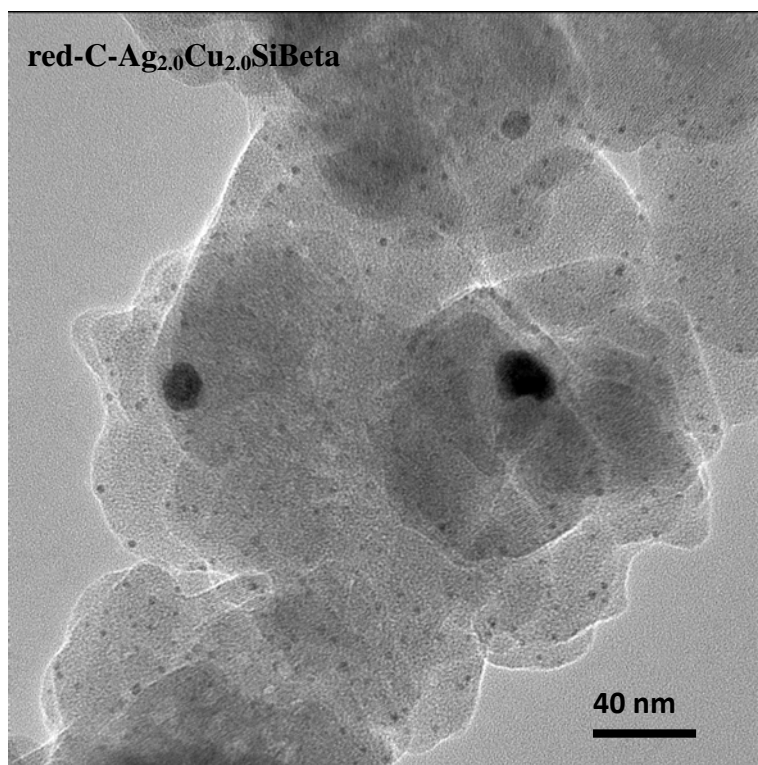


Figure 7

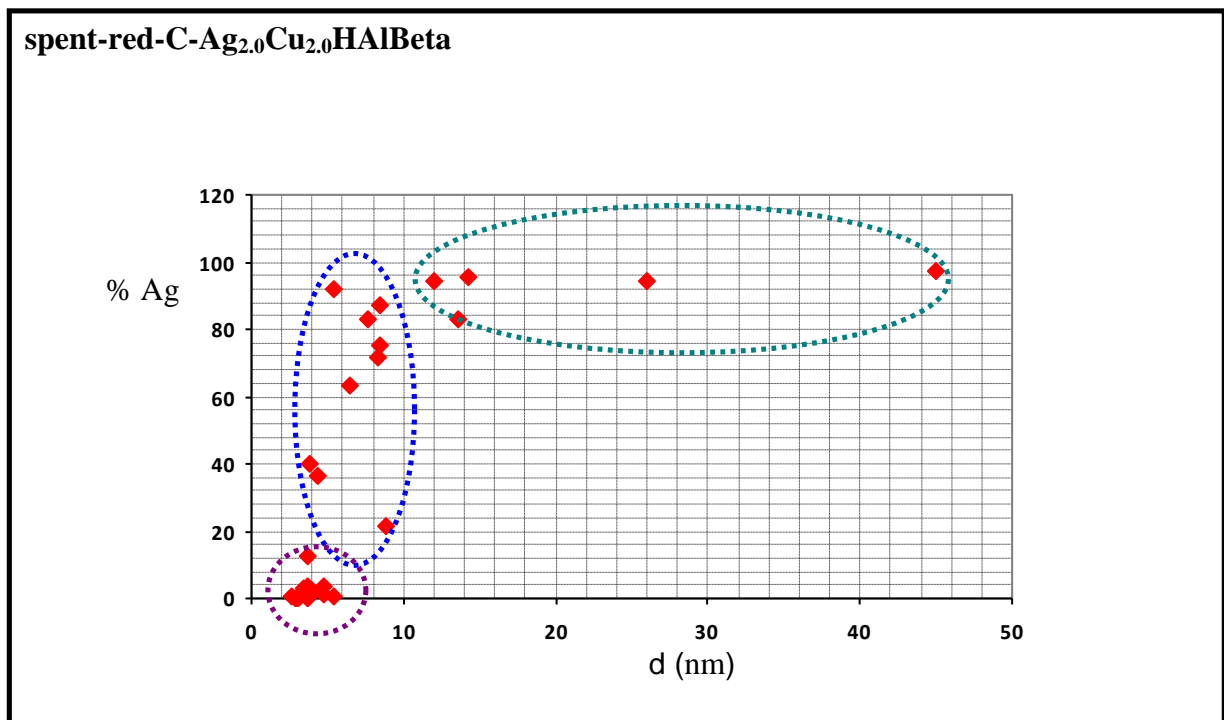
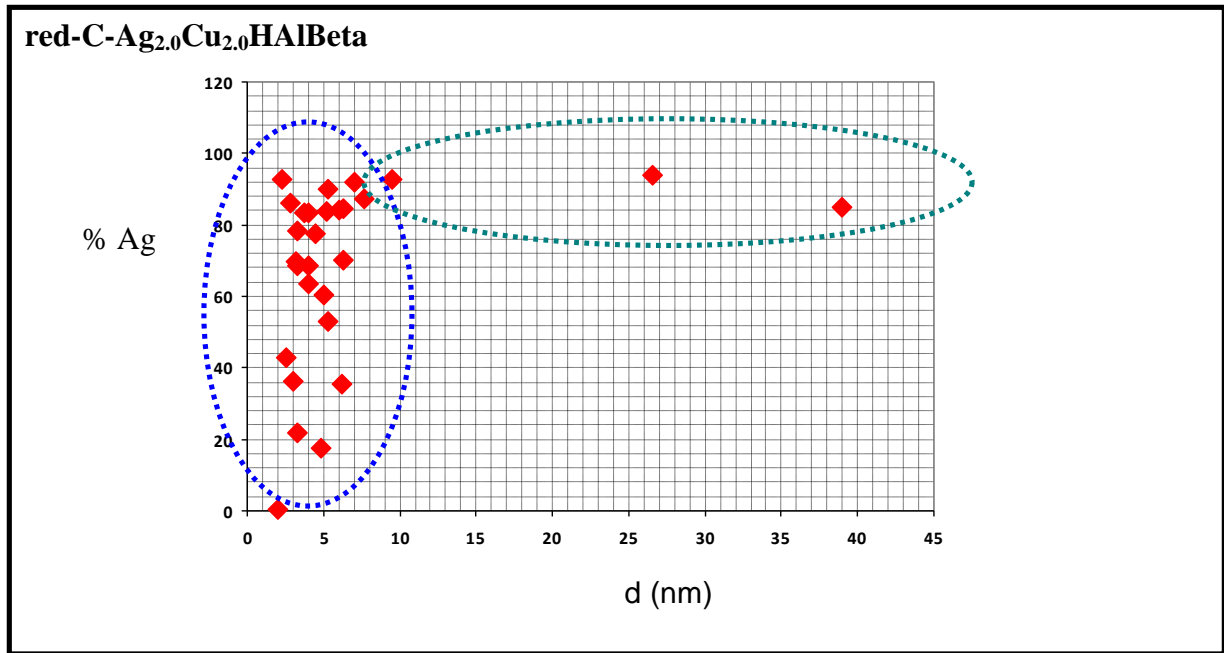


Figure 8

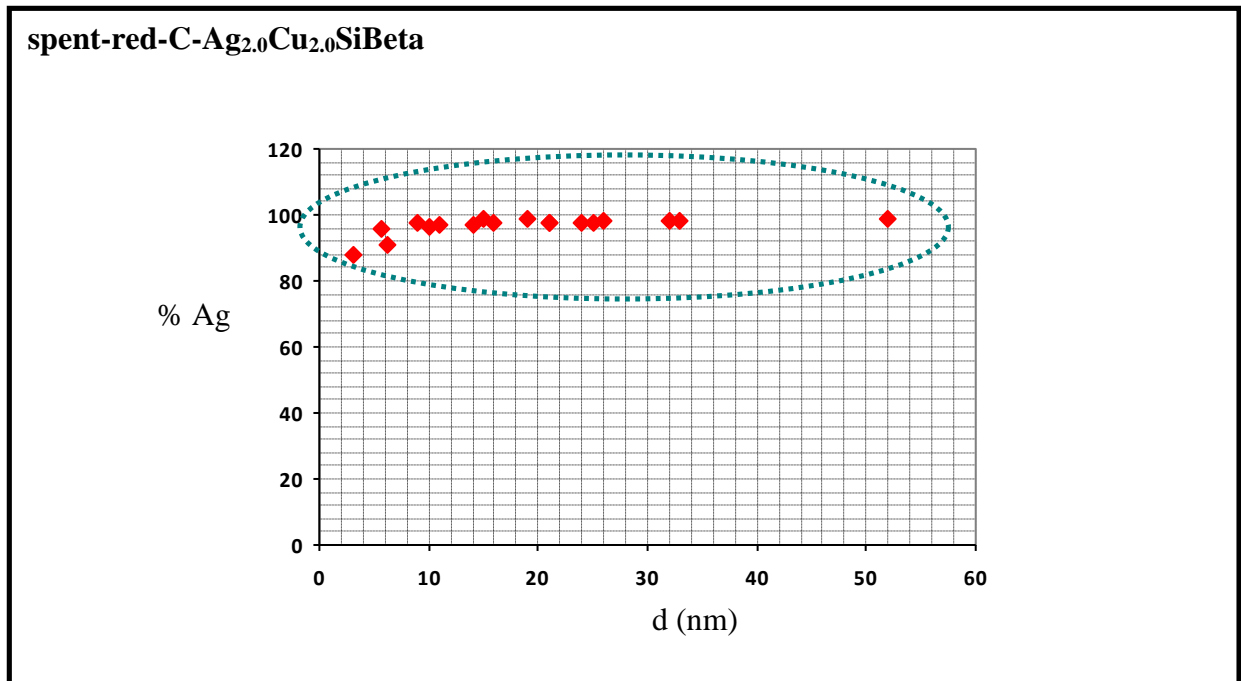
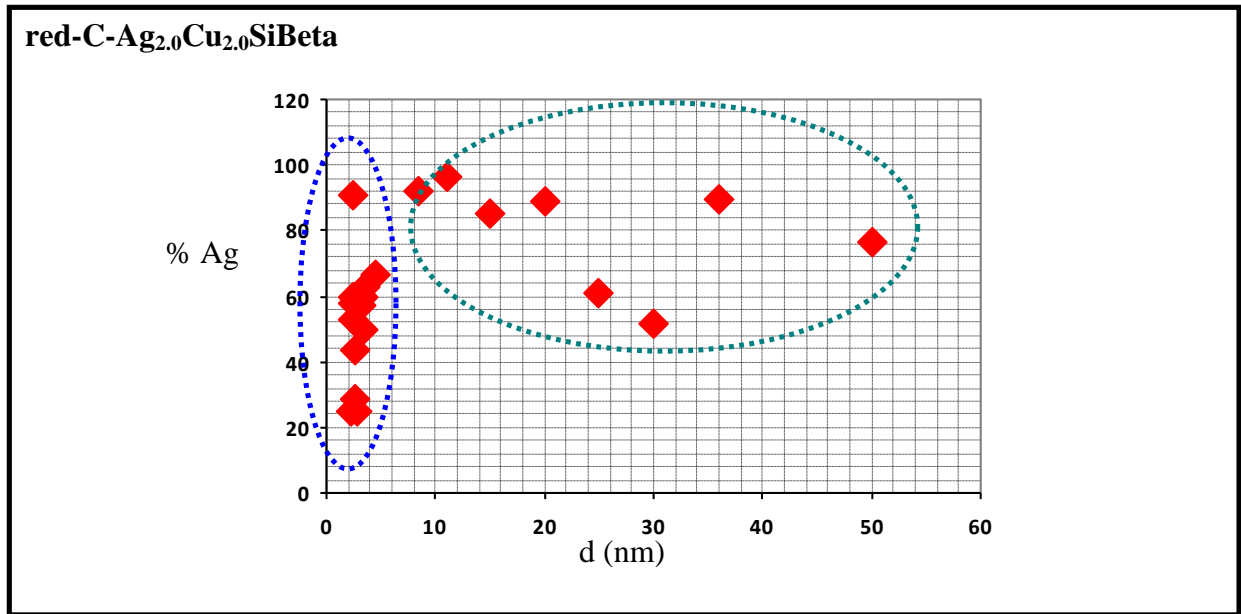


Figure 9

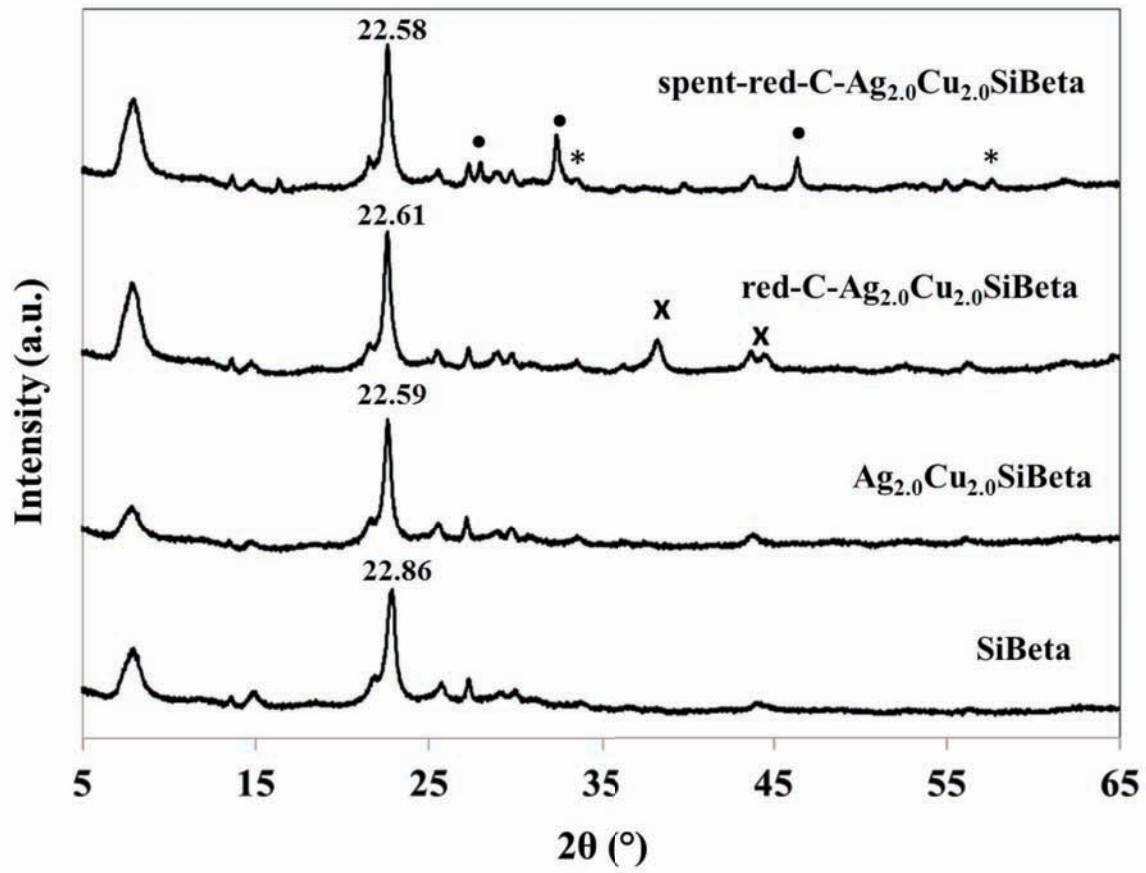


Figure 10

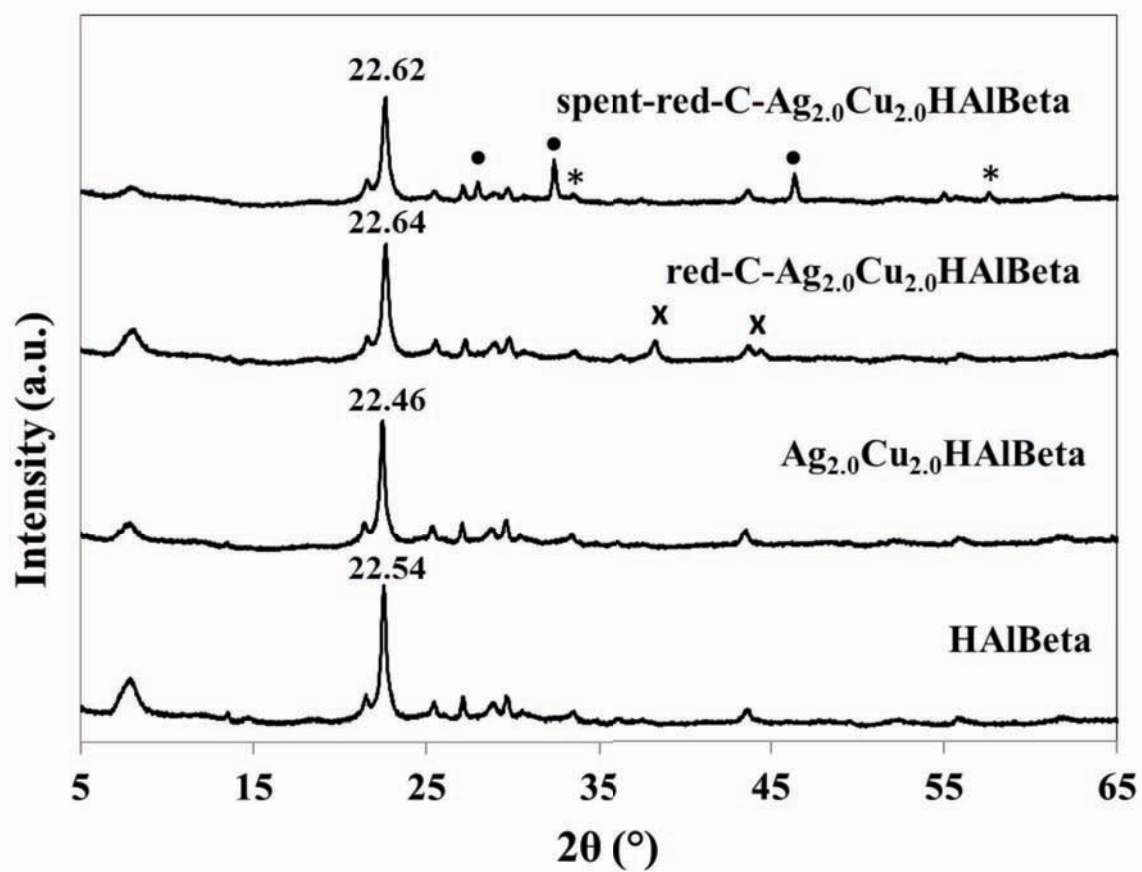


Figure 11

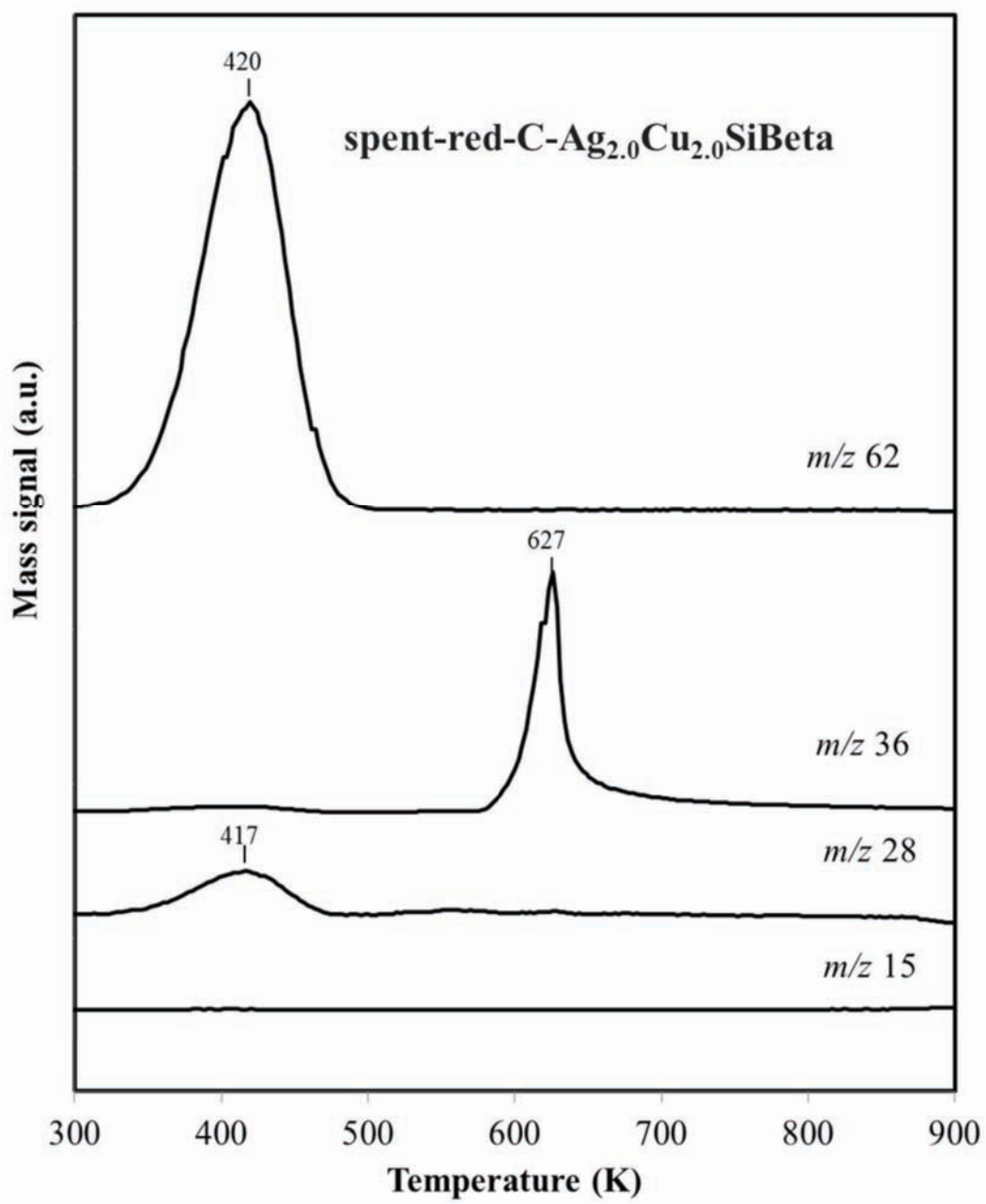


Figure 12

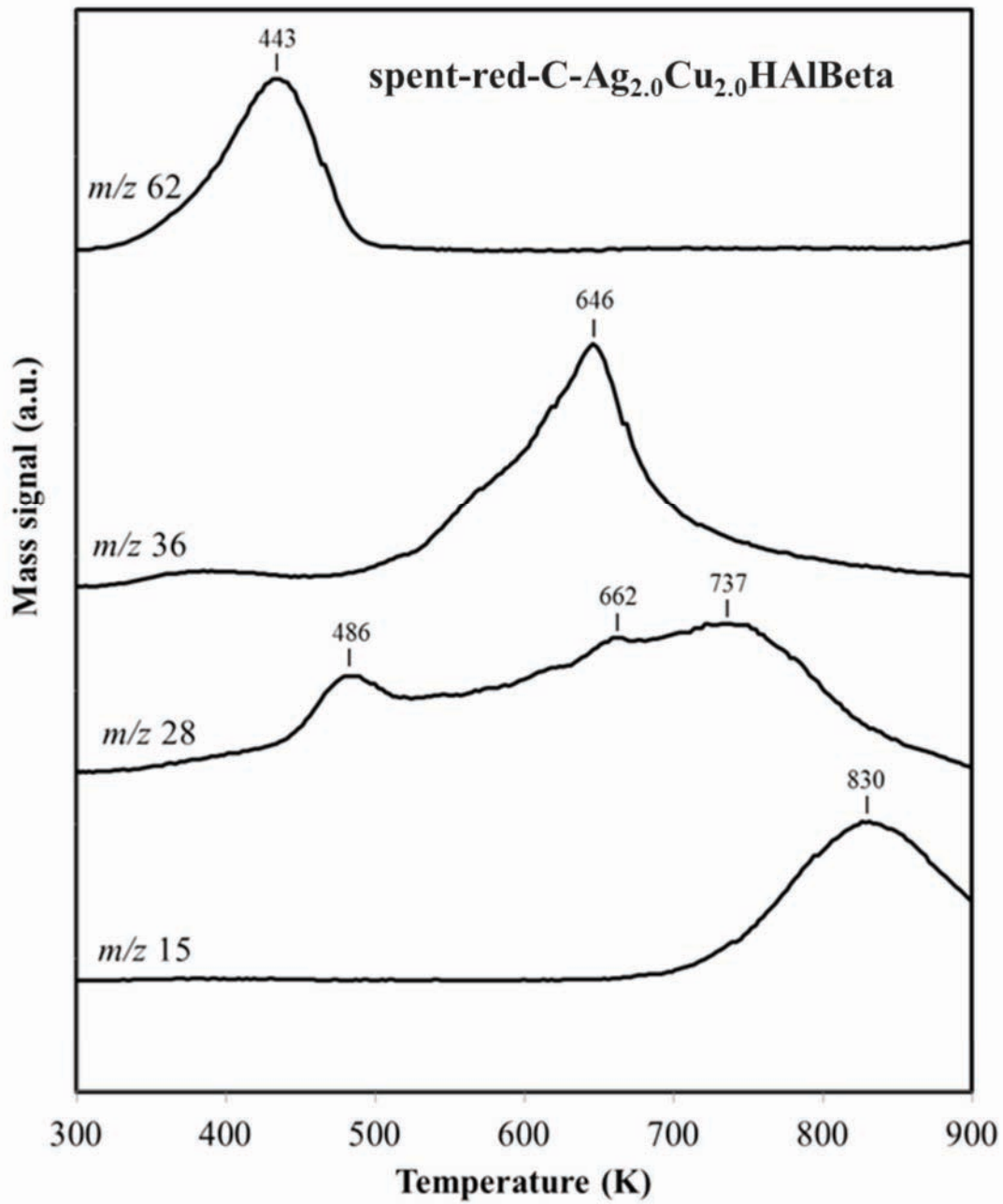


Figure 13

Highlights:

- Two-step postsynthesis method leads to formation small Ag and Cu nanoparticles.
- Vinyl chloride and/or ethylene are the main products of HDC of 1,2-dichloroethane.
- During HDC Ag and Cu nanoparticles agglomerate and transform into AgCl and CuCl₂.